iScience

CellPress
OPEN ACCESS

Article

Identification and verification of the role of key metabolites and metabolic pathways on ASFV replication

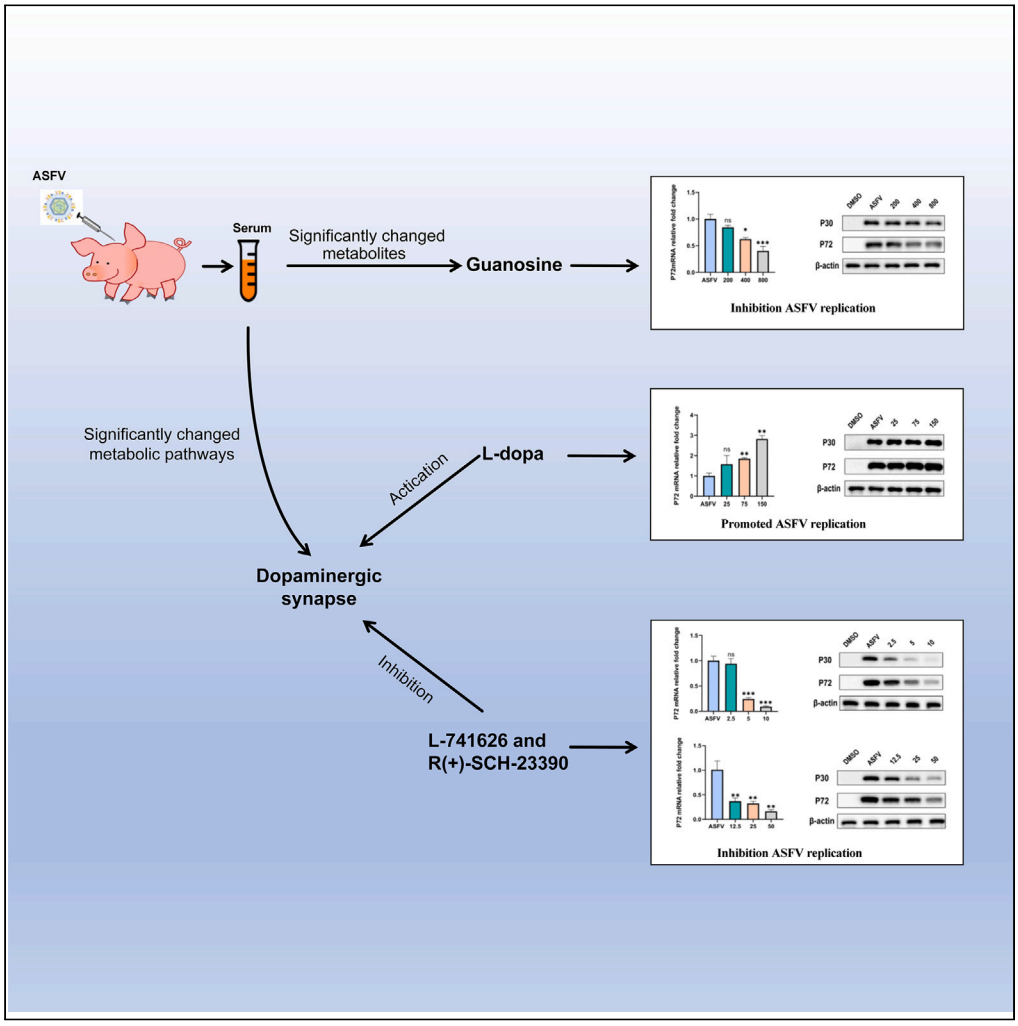

Zunji Shi, Xing Yang, Xijuan Shi, ..., Xiangtao Liu, Haixue Zheng, Keshan Zhang

zhenghaixue@caas.cn (H.Z.)
zks009@126.com (K.Z.)

Highlights

Revealed the metabolic changes in serum after ASFV infection

The key metabolites and metabolic pathways during ASFV infection were identified

The dopamine synaptic pathway can promote ASFV replication

Guanosine inhibited ASFV replication

Shi et al., iScience 27, 109345
April 19, 2024 © 2024
https://doi.org/10.1016/j.isci.2024.109345

iScience

CellPress
OPEN ACCESS

Article

Identification and verification of the role of key metabolites and metabolic pathways on ASFV replication

Zunji Shi,[1,2,4] Xing Yang,[1,4] Xijuan Shi,[1] Dajun Zhang,[1] Dengshuai Zhao,[1] Yu Hao,[1] Jinke Yang,[1] Xintian Bie,[1] Wenqian Yan,[1] Guohui Chen,[1] Lingling Chen,[1] Xiangtao Liu,[1] Haixue Zheng,[1,*] and Keshan Zhang[1,2,3,5,*]

SUMMARY

African swine fever virus (ASFV) infection usually causes viremia within a few days. However, the metabolic changes in pig serum after ASFV infection remain unclear. In this study, serum samples collected from ASFV-infected pigs at different times were analyzed using pseudotargeted metabolomics method. Metabolomic analysis revealed the dopaminergic synapse pathway has the highest rich factor in both ASFV5 and ASFV10 groups. By disrupting the dopamine synaptic pathway, dopamine receptor antagonists inhibited ASFV replication and L-dopa promoted ASFV replication. In addition, guanosine, one of the top20 changed metabolites in both ASFV5 and ASFV10 groups suppressed the replication of ASFV. Taken together, this study revealed the changed serum metabolite profiles of ASFV-infected pigs at various times after infection and verified the effect of the changed metabolites and metabolic pathways on ASFV replication. These findings may contribute to understanding the pathogenic mechanisms of ASFV and the development of target drugs to control ASF.

INTRODUCTION

African swine fever (ASF) is caused by the African swine fever virus (ASFV) characterized by high fever, cyanosis of the skin, and severe hemorrhages in the lymph nodes and other organs for both domestic and wild swine.[1] ASF was first reported in Kenya in 1921.[2] Nevertheless, its epidemics was started in the Caucasian region and rapidly spread to Europe and Asia.[3,4] ASF happened in China in Liaoning province in 2018.[5] The morbidity and mortality of ASF are very high, nearly to 100%. As the country which has the largest stock of pigs and the most pork consumption all over the world, ASFV had caused devastating influence and tremendous financial loss in the swine industry and economic trade.[1,6] ASFV is the sole member of the *Asfarviridae* family and the only known DNA arbovirus.[7] ASFV is an enveloped virus, with a large dsDNA genome of about 170–190 kbp, encoding more than 150 genes.[8,9] Up to date, effective information about ASFV infection and immune mechanisms during ASFV infection remained limited and the research on vaccines and drugs against ASFV was restricted.[10,11]

In the past decades, researches were devoted to focusing on protein pathogenesis encoded by ASFV. These proteins help complete self-replication and evade immune response in many ways. ASFV encodes several unique multigene families (MGFs): MGF100, MGF110, MGF300, MGF360, and MGF505.[12] The MGFs involved multiaspect during ASFV infection, including virulence, pathogenicity, host range, and immune evasion.[13,14] MGF-505-7R,[15,16] MGF505-11R,[17] MGF360-14L,[18] and MGF360-12L[19] have been reported suppress IFN-I production.[15–19] ASFV MGF360-9L can inhibit IFN-β signal pathway, through interacts with and degrading STAT1/2.[20] DP96R, pI215L, and E120R can negatively regulate cGAS-STING signaling pathway to suppressed interferon production.[21–23] ASFV genomic DNA can be recognized by DNA-directed RNA polymerase III (Pol-III) and induced RIG-I mediated innate immune responses, but I267L disrupted Pol-III-RIG-I interaction and impaired the activation of RIG-I.[24] Subsequently, pE199L induced mitochondrial-dependent apoptosis, which plays an important role in ASFV pathogenesis.[25] ASFV pH240R is a structural protein that interacts with p72 (major capsid protein), deleted *H240R* gene affected viral assembly and decreased infectious progeny virus production.[26] As aforementioned, most of these were concerning the protein-protein interaction. The intrinsic mechanisms underlying the interaction between ASFV and pigs remain largely unclear.

Metabolome technology can capture global changes in small molecule metabolites in biofluids, cells and tissues.[27] Small molecule metabolites are the substrates and products of metabolism that drive essential cellular functions.[28] Viral infection can reprogram host metabolism to

[1]State Key Laboratory for Animal Disease Control and Prevention, College of Veterinary Medicine, Lanzhou University, Lanzhou Veterinary Research Institute, Chinese Academy of Agricultural Sciences, Lanzhou 730000, China
[2]State Key Laboratory of Herbage Improvement and Grassland Agro-ecosystems, Center for Grassland Microbiome, College of Pastoral Agriculture Science and Technology, Lanzhou University, Lanzhou 730000, China
[3]Present address: Lanzhou Veterinary Research Institute, Chinese Academy of Agricultural Sciences, No. 1, Xujiaping, Lanzhou 730046, P.R. China
[4]These authors contributed equally
[5]Lead contact
*Correspondence: zhenghaixue@caas.cn (H.Z.), zks009@126.com (K.Z.)
https://doi.org/10.1016/j.isci.2024.109345

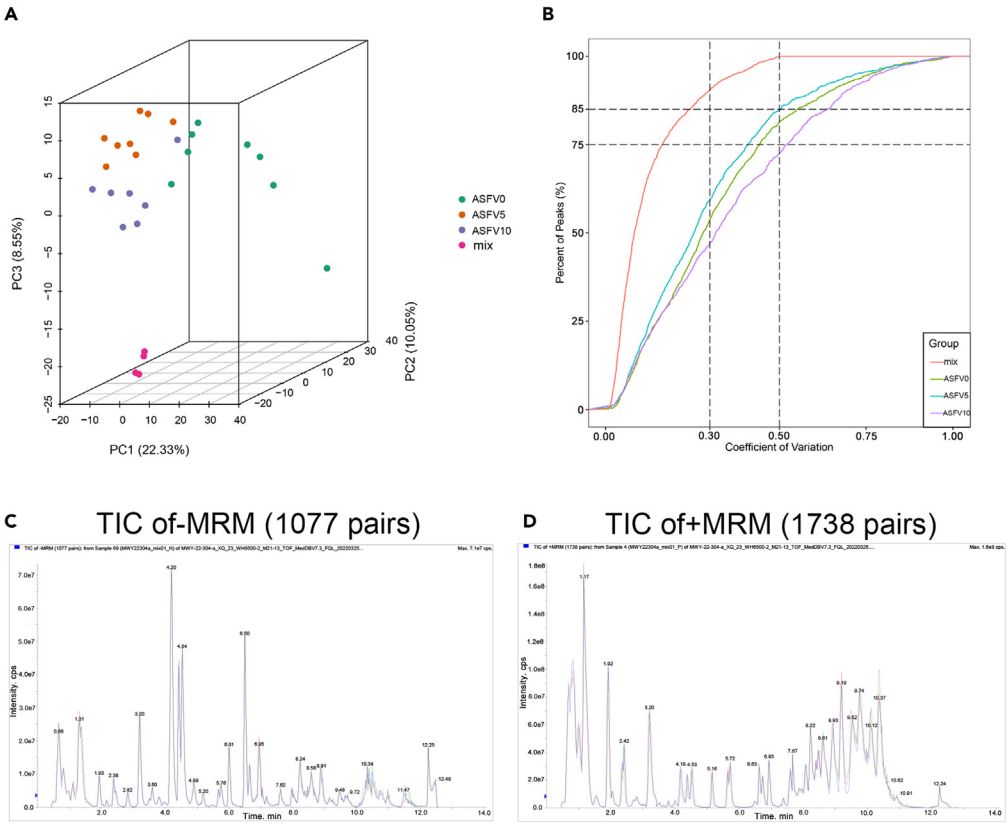

Figure 1. QC chart of LC-MS test data

(A) Overall score scatter diagram of PCA model: green represented ASFV infected 0dpi, blue represented ASFV infected 5dpi, red represented ASFV infected 10 dpi, and yellow represented mixed samples.

(B) CV distribution of samples: red represented mix samples, the same amount of ASFV infected 0 dpi, 5dpi, and 10 dpi samples were mixed as a QC, green represented serum of ASFV infected 10dpi, blue represented serum of ASFV infected 5dpi, and purple represented serum of ASFV infected 0 dpi, (C) TIC overlap diagram in positive ion mode (D) TIC overlap diagram in negative ion mode.

facilitate its replication and survival. Therefore, the changes of metabolites directly reflect the physiological and pathological status of humans and animals. In recent years, the metabolome analysis of host serum has gradually become a promising tool to determine the host-virus interaction *in vivo* and find biomarker for diagnosis.[29,30] The global serum metabolomics profiling during virus infection have been studied and reported, including severe acute respiratory syndrome coronavirus (SARS-CoV-2),[31] dengue virus (DENV),[32] human immunodeficiency virus-1 (HIV-1),[33] hepatitis C virus (HCV),[34] hepatitis B virus (HBV),[35] influenza A H7N9 virus(IAV H7N9),[36] and classical swine fever virus (CSFV).[37] These studies highlighted the huge potential of serum metabolomics in viral pathogenesis and detection. However, pig serum metabolomics during ASFV infection have not been fully elucidated yet.

Previous study of our research team analyzed the metabolism profiles of ASFV-infected PAM_S, showed that ASFV infection altered host energy and amino acid metabolism to promote viral replication, and induced lactate production increases to inhibit host innate immune responses.[38] In this study, for further explore the host response to ASFV, we inoculated pigs with ASFV CN/GS/2018, and collected serum samples for metabolomics analysis. ASFV infection significantly changed the metabolites in serum. We showed the global metabolites changes *in vivo* and investigated the influence on ASFV replication of changed metabolic pathway and metabolites. Taken together, our work revealed the status of ASFV-infected pigs from a metabolic perspective and provided new insights in ASFV infection process and pathogenic mechanism.

RESULTS

Serum metabolic profiling of all samples

The serum samples collection from all pigs at different time (0 dpi, 5dpi, and 10 dpi) were subjected to metabolomics analysis. A total of 1313 metabolites were detected using hydrophilic and hydrophobic methods by UHPLC-TQMS. The PCA (principal component analysis) result showed that the QC samples were clustered together, indicating the stability of this analytic method (Figure 1A). The majority of metabolic peaks had coefficients of variation less than 0.5, suggesting the reliability of the measurement technique (Figure 1B). In addition, the method

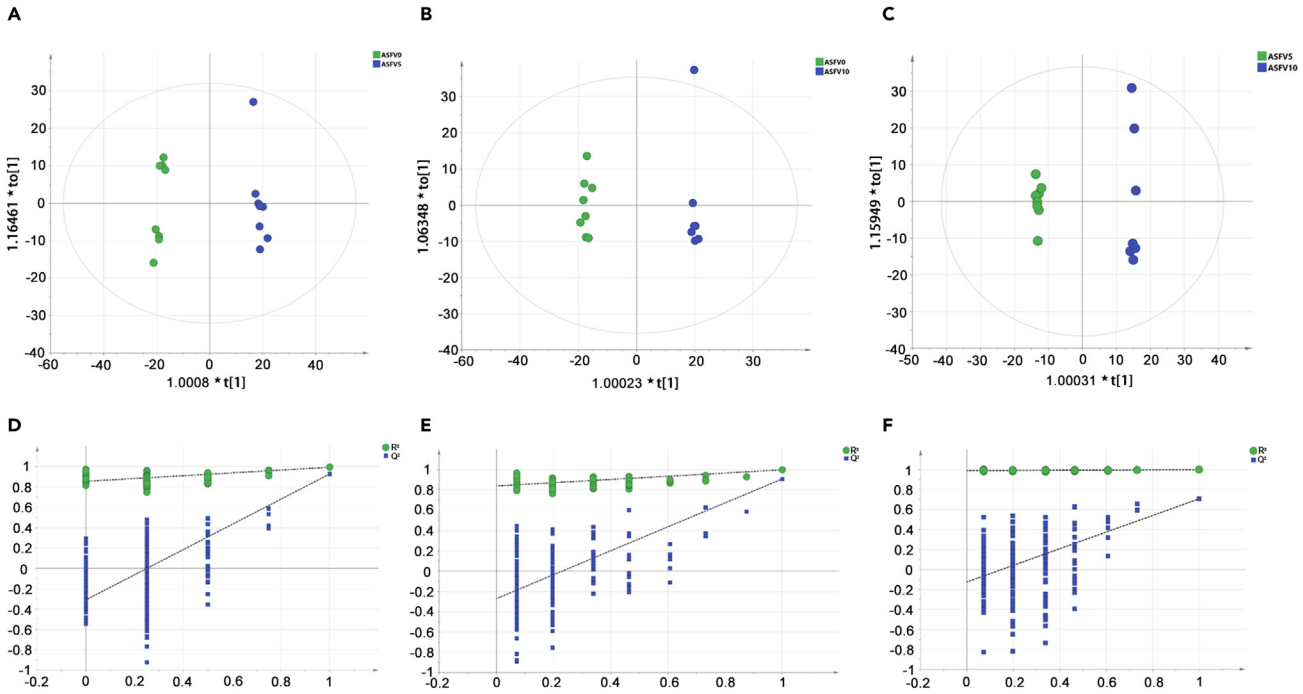

Figure 2. OPLS-DA model sequencing verification diagram

(A) OPLS-DA model score between ASFV5 and ASFV0.

(B) OPLS-DA model score between ASFV10 and ASFV0.

(C) OPLS-DA model score between ASFV10 and ASFV5. OPLS–DA model's permutation tests between ASFV5 and ASFV0 (D), between ASFV10 and ASFV0 (E), between ASFV10 and ASFV5 (F). R^2 and Q^2, respectively, represented the interpretation rate of the model to the matrix and the prediction ability of the model. The closer the value was to 1, the more stable and reliable the model was. The horizontal line corresponds to R^2 and Q^2 of the original model. Green and blue dots represented R^2 and Q^2 of the model after Y was replaced.

stability was assessed by overlaying different samples' total ion current diagrams (TIC diagrams). The results showed that the curves of the TIC diagrams were highly overlapped, and the retention time and peak intensity were consistent, demonstrating that the signals were stable throughout the analysis process (Figures 1C and 1D).

Metabolomics analysis of serum metabolites

We used the score plots of OPLS-DA (orthogonal partial least structures discriminant analysis) and permutation test model to visualize and verify the metabolite differences between groups (Figure 2). The PCA score plots revealed differences in metabolites among different days after ASFV infection (Figure 1A). The score plots of OPLS-DA showed a clear separation between ASFV0 (ASFV infected 0 dpi) and ASFV5 (ASFV infected 5 dpi) groups ($R^2X = 0.408$, $Q^2 = 0.927$), indicating that the model was reliable and had the good predictive ability (Figure 2A). The separation can also be seen between ASFV0 and ASFV10 (ASFV infected 10 dpi) groups, between ASFV5 and ASFV10 groups ($R^2X = 0.399$, $Q^2 = 0.907$; $R^2X = 0.397$, $Q^2 = 0.707$) (Figures 2B and 2C). R^2X represented the cumulative explanatory rate of the model in the X axis direction and Q^2 represented the cumulative prediction rate of the model when modeling the multivariate statistical analysis. The validity of these models was further confirmed by 200 permutation tests (Figures 2D–2F).

Comparison of serum metabolic profiling between the ASFV5 and ASFV0 groups

Firstly, to identify the changes of metabolites after 5 days of ASFV infection, we focused on the differential metabolites between ASFV5 and control (ASFV0) (Table S1). We performed a univariate t-test analysis based on the fold changes of metabolites in the two groups and found 290 metabolites with p value <0.05, FC $\geq$ 1.5 or $\leq$0.67, and VIP>1, in which 225 metabolites decreased and 65 metabolites increased in ASFV5, as shown in the volcano plot (Figure 3A). Besides, KEGG (Kyoto Encyclopedia of Genes and Genomes) pathway enrichment analysis of differential metabolites showed that there were mainly 20 significantly disturbed metabolic pathways (Figure 3B). Renin secretion metabolism, dopaminergic synapse metabolism, and african trypanosomiasis metabolism had the highest rich factor, and metabolic pathways metabolism had a maximum number of differential metabolites (Figure 3B). The top20-fold change distribution plot (Figure 3C) and barchart (Figure 3D) showed 10 upregulated metabolites in ASFV5 including senecionine N-oxide, ammelide, 3-hydroxyethylchlorophyllide, uridine, allopurinol, guanine, 2-hydroxy-6-aminopurine, guanosine, carnitine C10:0, and Lys-Ile, and 10 downregulated metabolites in ASFV5 including taurocholic acid, liquiritin, cyclo (Tyr-Ala), L-2-aminoadipate, baicalin, 12,13-dihome, khelloside, astragalin, and 3,4,2′,4′,6′-pentahydroxychalcone.

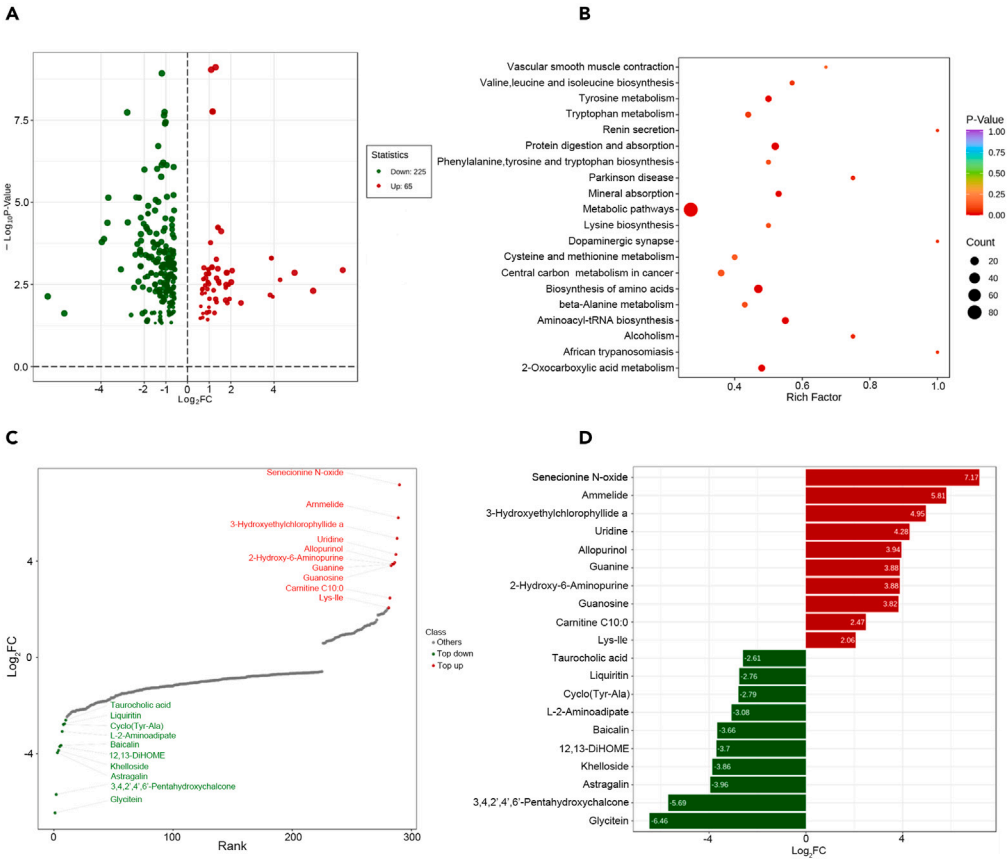

Figure 3. Differential metabolite analysis of ASFV0 VS ASFV5

(A) Volcano map between ASFV5 and ASFV0, green dots represented decreased differentially expressed metabolites, red dots represented increased differentially expressed metabolites.

(B) KEGG enrichment analysis of differential metabolites. The X axis represents the rich factor, and the Y axis represents the pathway. Each bubble represents a metabolic pathway and the bubble with larger represents more bubbles indicating a larger number of enriched metabolites enriched. A darker red color indicates a more significant enrichment; the top 20 metabolic pathways with the highest significance are shown.

(C) Dynamic distribution map of differences in metabolite content. Each point represented one metabolite, red represented top10 increased metabolites, green represented top10 decreased metabolites.

(D) Top20-fold change bar chart, exhibited the top10 most significantly upregulated or decreased metabolites. Red represented increased metabolites, green represented decreased metabolites.

Comparison of serum metabolic profiling between the ASFV10 and ASFV0 groups

Furthermore, special attention was given to the changes of metabolites after 10 days of ASFV infection, we focused on the differential metabolites between ASFV10 and control (ASFV0) (Table S2). A univariate t-test analysis based on the fold changes of metabolites was performed in the two groups and found 312 metabolites with p value <0.05, FC ≥ 1.5 or ≤0.67, and VIP>1, in which 254 metabolites decreased and 58 metabolites increased in ASFV10, as shown in the volcano plot (Figure 4A). Besides, KEGG enrichment analysis of differential metabolites showed that vitamin B6 metabolism, thyroid hormone signaling pathway metabolism, dopaminergic synapse metabolism, and autoimmune thyroid disease metabolism had the highest rich factor, and metabolic pathways metabolism had a maximum number of differential metabolites (Figure 4B). The top20-fold change distribution plot (Figure 4C) and barchart (Figure 4D) showed 10 upregulated metabolites in ASFV10 including 3-hydroxyethylchlorophyllide, senecionine N-oxide, ammelide, 2′-deoxyinosine, guanosine, allopurinol, guanine, 2-hydroxy-6-aminopurine, (±)5(6)-dihete, and carnitine C18:0, and 10 downregulated metabolites in ASFV10 including MG(22:6/0:0/0:0), 1,2-epoxy-3-(*p*-nitropheoxy) propane, 12,13-dihome, N-methyl-4-aminobutyric acid, liquiritin, baicalin, khelloside, astragalin, chrysophanol, and glycitein.

Comparison of serum metabolic profiling between the ASFV10 and ASFV5 groups

In addition, the differential metabolites between ASFV10 and ASFV5 were identified and analyzed (Table S3). A univariate t-test analysis based on the fold changes of metabolites was performed in the two groups and found 100 metabolites with p value <0.05, FC ≥ 1.5 or ≤0.67, and

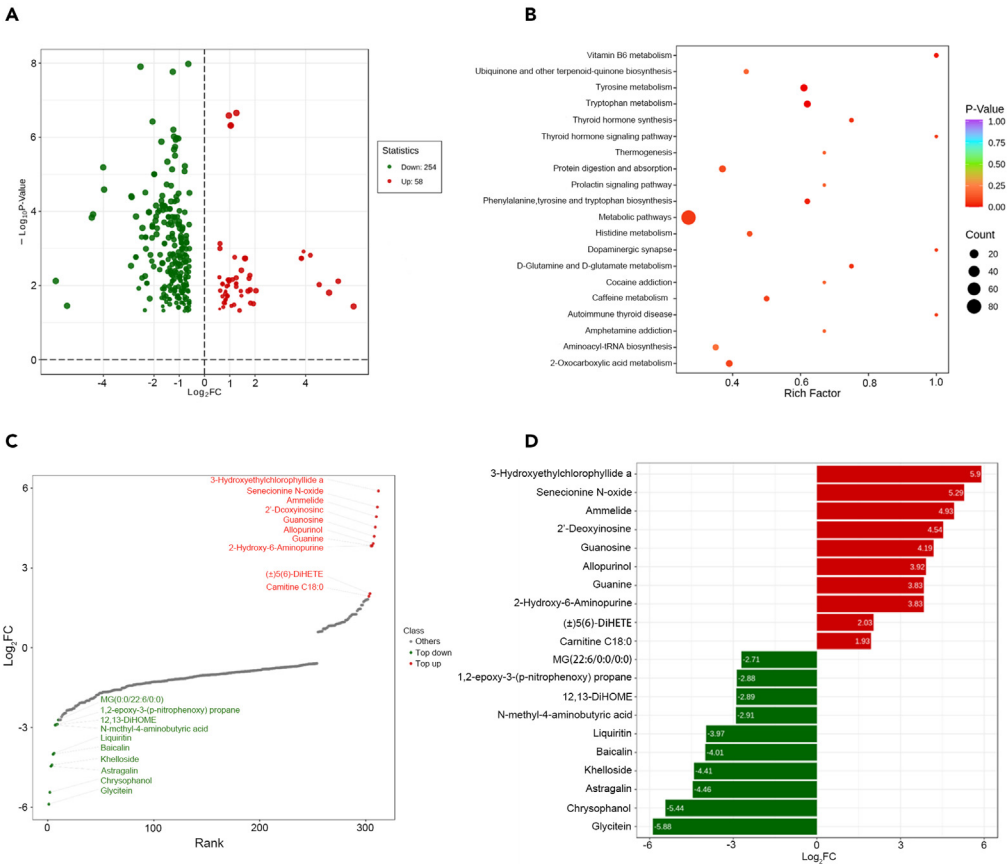

Figure 4. Differential metabolite analysis of ASFV10 VS ASFV0

(A) Volcano map between ASFV10 and ASFV0, green dots represented decreased differentially expressed metabolites, red dots represented increased differentially expressed metabolites.

(B) KEGG enrichment analysis of differential metabolites between ASFV10 and ASFV0.

(C) Dynamic distribution map of differences in metabolite content. Each point represented one metabolite, red represented top10 increased metabolites, green represented top10 decreased metabolites.

(D) Top20-fold change bar chart, exhibited the top10 most significantly upregulated or decreased metabolites. Red represented increased metabolites, green represented decreased metabolites.

VIP>1, in which 58 metabolites decreased and 42 metabolites increased in ASFV10, as shown in the volcano plot (Figure 5A). KEGG enrichment analysis of differential metabolites showed that retinol metabolism, thyroid hormone signaling pathway metabolism, and autoimmune thyroid disease metabolism had the highest rich factor, and biosynthesis of amino acids metabolism had a maximum number of differential metabolites (Figure 5B). The top20-fold change distribution plot (Figure 5C) and barchart (Figure 5D) showed 10 upregulated metabolites in ASFV10 including L-2-aminoadipate, *p*-hydroxyphenyl acetic acid, mandelic acid, N-methyl-*l*-glutamate, 2-aminoadipic acid, l-deprenyl, 3-hydroxyphenylacetic acid, beta-muricholic acid, alpha-muricholic acid, and piritramide, and 10 downregulated metabolites in ASFV10 including uridine, Gly-Ile, N-acetyl-beta-alanine, Tyr-Glu, Gly-Leu, N-acetyl-*l*-alanine, 2-amino-4-oxovaleric acid, Glu-His, anabaenopeptilide 90A, and senecionine N-oxide.

Impact of altered metabolites and metabolic pathways on ASFV replication

Metabolomics analysis of serum metabolites at different times after ASFV infection revealed the changes of metabolites and metabolic pathways. We found the dopaminergic synapse metabolism had the highest rich factor in between ASFV5 and ASFV0 (Figure 3B), between ASFV10 and ASFV0 (Figure 4B). To explore the effect of dopaminergic synapse metabolism on ASFV replication, the antagonist of dopamine receptor including L741626 and R (+)-SCH-23390 were selected to inhibit the dopaminergic synapse pathway. The cytotoxicity of L741626 and R (+)-SCH-23390 was determined on PAMs (porcine alveolar macrophages), which were cultured in 12-well plates infected with ASFV (MOI = 0.1) and treated with different gradient concentrations of L741626 or R (+)-SCH-23390. Two drugs had no significant cytotoxicity on PAMs (Figure 6A). The P30 and P72 protein levels of ASFV under different concentrations were analyzed via immunoblotting, and the P72 mRNA levels of ASFV under different concentrations were detected by qPCR. The results showed that L741626 and R (+)-SCH-23390

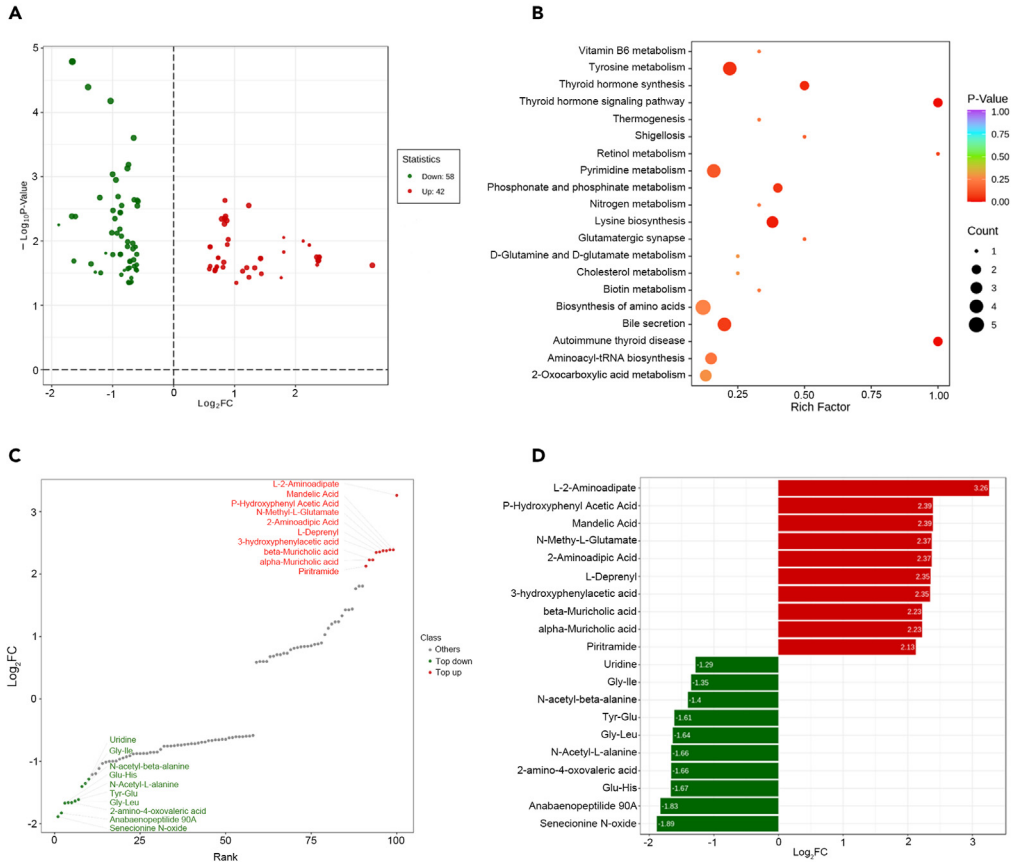

Figure 5. Differential metabolite analysis of ASFV10 VS ASFV5

(A) Volcano map of significantly changed metabolites between ASFV10 and ASFV5 (B) KEGG enrichment analysis of differential metabolites between ASFV10 and ASFV5.

(C) Dynamic distribution map of differences in metabolite content. Each point represented one metabolite, red represented top10 increased metabolites, green represented top10 decreased metabolites.

(D) Top20-fold change bar chart, exhibited the top10 most significantly upregulated or decreased metabolites. Red represented increased metabolites, green represented decreased metabolites.

inhibited ASFV replication in a dose-dependent manner (Figures 6B and 6C). L-dopa is the precursor of dopamine39. L-dopa did not cause significant cytoxicity (Figure 6A), and exogenous addition of different doses of L-dopa can significantly promote ASFV replication at viral protein and mRNA levels (Figures 6B and 6C).

To investigate the effect of significant changed metabolites on ASFV replication, we selected guanosine and allopurinol, which were top20 changed metabolites in between ASFV5 and ASFV0, between ASFV10 and ASFV0, for further validation experiments. Different concentrations of guanosine or allopurinol did not cause significant cytotoxicity in PAMs (Figure 6A). qPCR results showed that guanosine inhibited ASFV replication in a dose-dependent manner, but allopurinol had no marked impact on ASFV replication (Figure 6B). The expression of ASFV proteins (P30 and P72) exhibited the similar tendency (Figure 6C).

DISCUSSION

Today, ASFV is one of the most serious viral diseases in the pig industry in China.[39] Unfortunately, there are no effective drugs against ASFV yet. In the past decades, the researcher had made great progress in ASFV study, but the mechanism of ASFV-host interaction is still limited. To facilitate virus replication, virus regulation of host metabolism produces a large number of metabolites required for viral replication.[38,40,41] On the contrary, some metabolites of host also can inhibit virus infection.[42,43] Therefore, study on the influence of ASFV infection on host metabolism will be helpful to understanding its pathogenesis, and promote the development of vaccines and drugs. In the present study, we analyzed the serum metabolomics profiles of ASFV-infected pigs using UHPLC-TQMS. Our results showed that several metabolic pathways were disturbed, and revealed a novel insight of ASFV-host interaction *in vivo*, which may help the research and development of vaccines and drugs for ASFV.

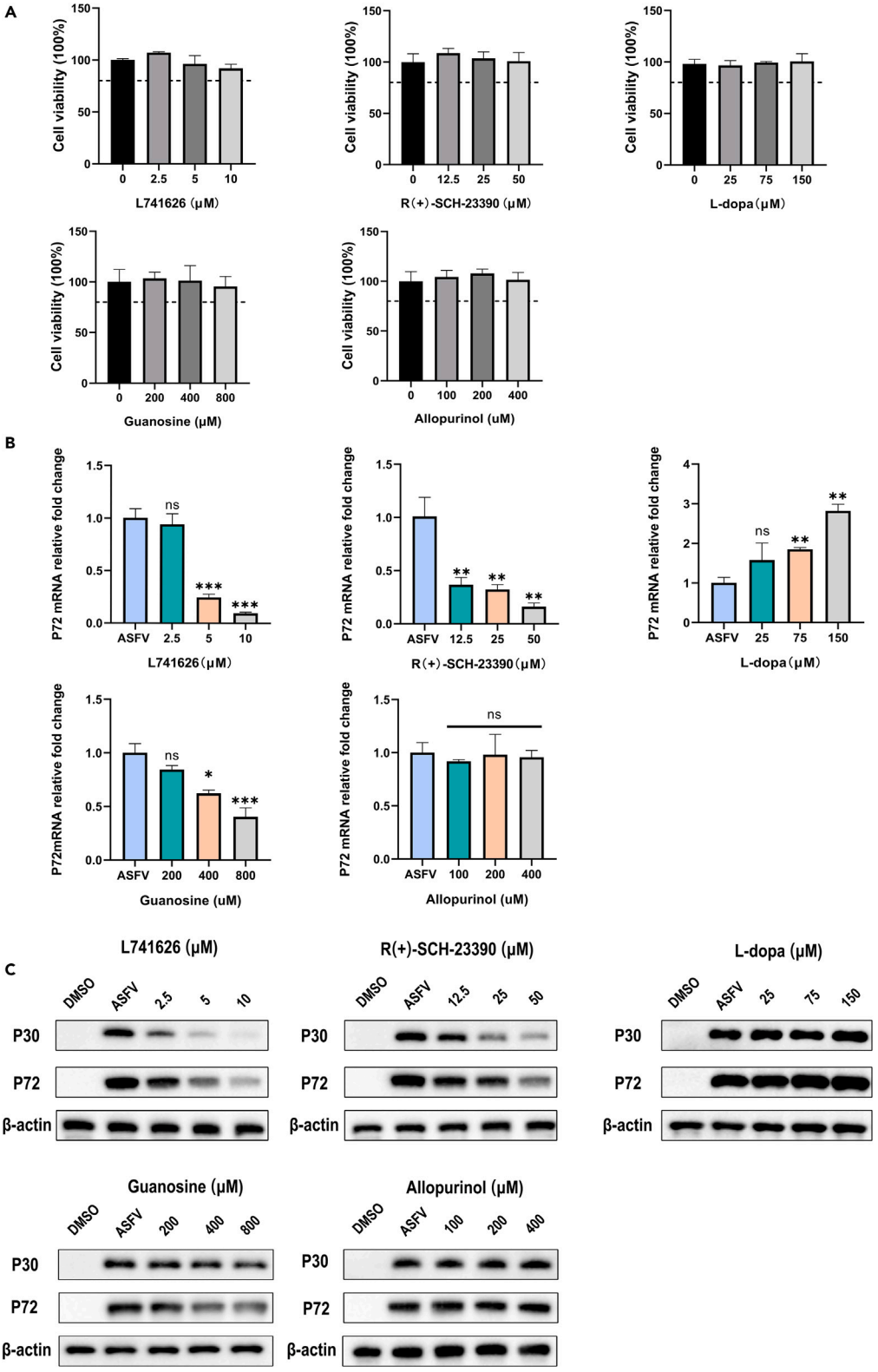
A
Cell viability (100%)
L741626 (μM)
R(+)-SCH-23390 (μM)
L-dopa(μM)
Guanosine (μM)
Allopurinol (uM)
B
P72 mRNA relative fold change
P72mRNA relative fold change
ns
ASFV
C
L741626 (μM)
R(+)-SCH-23390 (μM)
L-dopa (μM)
Guanosine (μM)
Allopurinol (μM)
DMSO
P30
P72
β-actin

Figure 6. Changed metabolites and metabolic pathway influence ASFV replication

(A) The cell cytotoxicity of metabolites and drugs were separate quantified using cell counting kit-8 (CCK-8) assay.

(B) Effects of metabolites and drugs on the viral RNA levels. PAMs were infected with equal amounts of ASFV (MOI = 0.1) and treated with increasing concentrations of metabolites and drugs. The same volume of DMSO or PBS was added as a mock infection. At 24 hpi, the viral RNA level was analyzed using RT-qPCR.

(C) Effects of metabolites and drugs on the expression of viral protein. As aforementioned, cell samples were prepared, the cell lysates were analyzed using western blotting via anti-P30 and anti-P72 antibodies.

Metabolites are closely correlated with host phenotype, because they are terminal products of gene expression.[44] Metabolomics exhibits the potential to determine the metabolic small molecules or the metabolic biomarkers related with disease pathogenesis, which may be not identified by proteomics and transcriptomics. Therefore, metabolomics exhibits the advantages to identify new and crucial metabolic pathways related to viral replication, and pathophysiology.[45] Metabolic pathways including TCA cycle, glycolysis, lipid biosynthesis, nucleotide, and amino acid metabolism pathways are probably affected by virus infections.[45] In the current study, OPLS-DA and permutation test model were used to visualize and exhibit the significant alteration of metabolites between groups. Further, the differential metabolites and associated KEGG enrichment pathways in serum after ASFV infection were identified through the comparison with the control group. Rich factor indicated the ratio of the number of significant changed metabolites to all metabolites in the pathway, and a higher rich factor indicates greater enrichment degree.[46] Our results showed that vitamin B6 metabolism, thyroid hormone signaling pathway metabolism, dopaminergic synapse metabolism, autoimmune thyroid disease metabolism, renin secretion metabolism, and African trypanosomiasis metabolism have the highest rich factor. Further, dopaminergic synapse metabolism has the highest rich factor in both ASFV5 vs. ASFV0 and ASFV10 vs. ASFV0. Dopamine, a neurotransmitter, causing signal transduction that binds to DA receptors.[47] Previous research reported dopamine and the agonist of dopamine receptor promoted HIV replication.[48] However, L-dopa (precursors of dopamine) has been reported inhibited SARS-COV-2,[49] HCV,[50] and DENV[51] replication. In this study, exogenous addition experiments of L-dopa and dopamine receptor antagonists further validated that the dopaminergic synapse metabolism was essential for ASFV replication. Dopamine is a key metabolite of dopamine metabolism, whose regulation of innate immunity has been reported in previous study.[52] Epinephrine, the product of dopamine metabolism, can inhibit innate immune through PKA inhibiting MITA and VISA activation.[53] It is possible that the dopaminergic synapse metabolism pathway can negatively regulate innate immunity for promoting ASFV replication, but the specific mechanism still needs further research.

Amino acids are used to synthetize protein and provide primary metabolic substances. Previous studies indicated that amino acids metabolism was markedly affected by viral infection.[40,54,55] Our research team previously indicated that ASFV infection altered amino acids metabolism to promote viral replication in PAMs.[38] In the current study, we found that several KEGG enrichment pathways associated with amino acids metabolism was markedly altered after ASFV infection, including biosynthesis of amino acids, lysine biosynthesis, tyrosine metabolism, valine, leucine and isoleucine biosynthesis, tryptophan metabolism, histidine metabolism, phenylalanine, tyrosine, and tryptophan biosynthesis. Moreover, the amino acid contents of serum samples from different time after ASFV infection showed no significant change. However, the results of serum metabolic profiling exhibited several amino acids were markedly increased at 5 and 10 days after ASFV infection, including N-methylisoleucine, L-cystine, L-asparegine anhydrous. More amino acids were significantly reduced at 5 and 10 days after ASFV infection, including L-ornithine, L-threonine, L-methionine, methylcysteine, L-tryptophan, L-Lysine, L-glutamine, Pytoglutamic, and L-theanine. It's interesting that the content of L-lysine and L-glutamine were markedly increased in ASFV-infected 10 days compared to ASFV-infected 5 days (Figure S1).

In addition to amino acids, viruses need to use nucleotides provided by host cells for viral replication. The alteration of nucleotides metabolism was markedly induced by viral infection, which included newcastle disease virus, H1N1 influenza virus, influenza virus, COVID-19, and so on.[40,56–58] In the current study, top20-fold change distribution plot showed that several metabolites including guanine, guanosine, 2-hydroxy-6-aminopurine, and allopurinol associated with nucleotides metabolism were markedly increased after ASFV5 and ASFV10 infection. Previous study showed that reported guanosine inhibits HCV replication by modified the di- and tri-phosphates (NDPs and NTPs).[59] Allopurinol is a potent antioxidant through inhibition an essential enzyme of purine metabolism (xanthine oxidase, XO), and can significant amelioration the clinical outcomes of COVID-19.[60] Thus, allopurinol and guanosine were selected to verify the effect of nucleotide metabolites on ASFV replication. In this study, allopurinol did not affect ASFV replication, and guanosine significantly inhibited ASFV replication via western blot and RT-qPCR. The specific mechanism of guanosine inhibiting ASFV will become an important part of our future research.

Study on the influence of ASFV infection on host metabolism will be helpful to understand the knowledge gaps regarding viral pathogenesis, promoting the development of vaccines and drugs. In summary, this study analyzed the serum metabolomics profiles of ASFV-infected pigs using UHPLC-TQMS, visualizing and exhibiting the significant alteration of metabolites between groups by OPLS-DA and permutation test model. The differential metabolites and associated KEGG enrichment pathways in serum after ASFV infection were identified, and several pathways associated with amino acids metabolism were markedly altered after ASFV infection. In addition, dopaminergic synapse pathway is crucial for ASFV replication. Top20-fold change distribution plot showed that several metabolites associated with nucleotides metabolism were markedly increased after ASFV5 and ASFV10 infection. Furthermore, guanosine, one top20 changed metabolites related to nucleotides metabolism, can inhibit ASFV replication. Our study will provide novel preventive strategies targeting the altered metabolic pathways, which may accelerate the development of vaccines and drugs for ASFV.

Limitations of the study

There are several notable limitations of our study. A key limitation of our study is that although we show inhibition dopamine synaptic pathway and exogenous addition guanosine reduced ASFV replication, we have not determined the specific mechanisms of dopamine and guanosine

inhibited ASFV replication. Another limitation of this study is we show dopamine receptor antagonist, L-dopa and guansine not cause significant cytotoxicity in PAMs, but how the PAMs respond to dopamine and guanosine is unclear. What's more, the sex of the experimental animals used in this study were all female, the influence of ASFV on metabolism in different sex animals are unclear. Future studies will be committed to exploring the impact of these metabolites on the pathogenesis and exploring their specific mechanisms.

STAR★METHODS

Detailed methods are provided in the online version of this paper and include the following:

- KEY RESOURCES TABLE
- RESOURCE AVAILABILITY
  - Lead contact
  - Materials availability
  - Data and code availability
- EXPERIMENTAL MODEL AND STUDY PARTICIPANT DETAILS
  - Cells
  - Animal experiments and samples collection
- METHOD DETAILS
  - Metabolite extraction
  - UHPLC-TQMS analysis
  - Western blotting
  - Real-time quantitative polymerase chain reaction (qPCR)
- QUANTIFICATION AND STATISTICAL ANALYSIS

SUPPLEMENTAL INFORMATION

Supplemental information can be found online at https://doi.org/10.1016/j.isci.2024.109345.

ACKNOWLEDGMENTS

This work was supported by grants from the National Key R&D Program of China (2021YFD1801300). This work was supported by the major science and technology project of Gansu Province, China (22ZD6NA001, 22ZD6NA012). The Research funding from National Swine Technology Innovation Center of China (NCTIP-XD/C03, CARS-35). This work was supported by the Institute of Animal Health, Guangdong Academy of Agricultural Sciences of China (2022SDZG02). The work was supported by the science and technology of Gansu Project (21JR7RA024), the Fundamental Research Funds for the Central Universities (lzujbky-2022-ct04). The authors are grateful to Metware Biotechnology Co., Ltd for their assistance in metabolomics analysis and Biogoethe Biotechnology (Wuhan) Co., Ltd for their contribution in the supply of reagent kits. The authors would like to thank all the editors and reviewers for their valuable comments and suggestions that helped improve the quality of this manuscript.

AUTHOR CONTRIBUTIONS

Z.S. and X.Y.: conceptualization. X.Y., X.B., and G.C.: formal analysis. K.Z. and H.Z.: funding acquisition. Z.S., Da.Z., and X.S.: investigation. K.Z.: supervision. X.Y., H.Y., De.Z., W.Y., and L.C.: validation. H.Y. and X.L.: writing—original draft. K.Z. and H.Z.: writing—review, and editing. All authors contributed to the article and approved the submitted version.

DECLARATION OF INTERESTS

The authors declare that the research was conducted in the absence of any commercial or financial relationships that could be construed as a potential conflict of interest.

Received: September 25, 2023
Revised: December 6, 2023
Accepted: February 22, 2024
Published: February 28, 2024

REFERENCES

1. Zhao, D., Liu, R., Zhang, X., Li, F., Wang, J., Zhang, J., Liu, X., Wang, L., Zhang, J., Wu, X., et al. (2019). Replication and virulence in pigs of the first African swine fever virus isolated in China. Emerg. Microbes Infect. *8*, 438–447. https://doi.org/10.1080/22221751.2019.1590128.
2. Eustace Montgomery, R. (1921). On A Form of Swine Fever Occurring in British East Africa (Kenya Colony). J. Comp. Pathol. Ther. *34*, 159–191. https://doi.org/10.1016/S0368-1742(21)80031-4.
3. Rowlands, R.J., Michaud, V., Heath, L., Hutchings, G., Oura, C., Vosloo, W., Dwarka, R., Onashvili, T., Albina, E., and Dixon, L.K. (2008). African swine fever virus isolate, Georgia, 2007. Emerg. Infect. Dis. *14*, 1870–1874. https://doi.org/10.3201/eid1412.080591.
4. Brookes, V.J., Barrett, T.E., Ward, M.P., Roby, J.A., Hernandez-Jover, M., Cross, E.M.,

Donnelly, C.M., Barnes, T.S., Wilson, C.S., and Khalfan, S. (2021). A scoping review of African swine fever virus spread between domestic and free-living pigs. Transbound. Emerg. Dis. *68*, 2643–2656. https://doi.org/10.1111/tbed.13993.

5. Wen, X., He, X., Zhang, X., Zhang, X., Liu, L., Guan, Y., Zhang, Y., and Bu, Z. (2019). Genome sequences derived from pig and dried blood pig feed samples provide important insights into the transmission of African swine fever virus in China in 2018. Emerg. Microbes Infect. *8*, 303–306. https://doi.org/10.1080/22221751.2019.1565915.
6. Vuono, E.A., Ramirez-Medina, E., Pruitt, S., Rai, A., Espinoza, N., Velazquez-Salinas, L., Gladue, D.P., and Borca, M.V. (2021). Evaluation of the Function of the ASFV KP177R Gene, Encoding for Structural Protein p22, in the Process of Virus Replication and in Swine Virulence. Viruses *13*, 986. https://doi.org/10.3390/v13060986.
7. Cuesta-Geijo, M.Á., García-Dorival, I., del Puerto, A., Urquiza, J., Galindo, I., Barrado-Gil, L., Lasala, F., Cayuela, A., Sorzano, C.O.S., Gil, C., et al. (2022). New insights into the role of endosomal proteins for African swine fever virus infection. PLoS Pathog. *18*, e1009784. https://doi.org/10.1371/journal.ppat.1009784.
8. Wang, N., Zhao, D., Wang, J., Zhang, Y., Wang, M., Gao, Y., Li, F., Wang, J., Bu, Z., Rao, Z., and Wang, X. (2019). Architecture of African swine fever virus and implications for viral assembly. Science *366*, 640–644. https://doi.org/10.1126/science.aaz1439.
9. Li, D., Wu, P., Liu, H., Feng, T., Yang, W., Ru, Y., Li, P., Qi, X., Shi, Z., and Zheng, H. (2022). A QP509L/QP383R-Deleted African Swine Fever Virus Is Highly Attenuated in Swine but Does Not Confer Protection against Parental Virus Challenge. J. Virol. *96*, e0150021. https://doi.org/10.1128/JVI.01500-21.
10. Wu, K., Liu, J., Wang, L., Fan, S., Li, Z., Li, Y., Yi, L., Ding, H., Zhao, M., and Chen, J. (2020). Current State of Global African Swine Fever Vaccine Development under the Prevalence and Transmission of ASF in China. Vaccines (Basel) *8*, 531. https://doi.org/10.3390/vaccines8030531.
11. Wang, Z., Ai, Q., Huang, S., Ou, Y., Gao, Y., Tong, T., and Fan, H. (2022). Immune Escape Mechanism and Vaccine Research Progress of African Swine Fever Virus. Vaccines (Basel) *10*, 344. https://doi.org/10.3390/vaccines10030344.
12. Zhu, Z., Chen, H., Liu, L., Cao, Y., Jiang, T., Zou, Y., and Peng, Y. (2021). Classification and characterization of multigene family proteins of African swine fever viruses. Brief. Bioinform. *22*, 380. https://doi.org/10.1093/bib/bbaa380.
13. Huang, L., Li, J., Zheng, J., Li, D., and Weng, C. (2022). Multifunctional pMGF505-7R Is a Key Virulence-Related Factor of African Swine Fever Virus. Front. Microbiol. *13*, 852431. https://doi.org/10.3389/fmicb.2022.852431.
14. Rathakrishnan, A., Connell, S., Petrovan, V., Moffat, K., Goatley, L.C., Jabbar, T., Sánchez-Cordón, P.J., Reis, A.L., and Dixon, L.K. (2022). Differential Effect of Deleting Members of African Swine Fever Virus Multigene Families 360 and 505 from the Genotype II Georgia 2007/1 Isolate on Virus Replication, Virulence, and Induction of Protection. J. Virol. *96*, e0189921. https://doi.org/10.1128/jvi.01899-21.
15. Li, D., Yang, W., Li, L., Li, P., Ma, Z., Zhang, J., Qi, X., Ren, J., Ru, Y., Niu, Q., et al. (2021). African Swine Fever Virus MGF-505-7R Negatively Regulates cGAS-STING-Mediated Signaling Pathway. J. Immunol. *206*, 1844–1857. https://doi.org/10.4049/jimmunol.2001110.
16. Li, J., Song, J., Kang, L., Huang, L., Zhou, S., Hu, L., Zheng, J., Li, C., Zhang, X., He, X., et al. (2021). pMGF505-7R determines pathogenicity of African swine fever virus infection by inhibiting IL-1beta and type I IFN production. PLoS Pathog. *17*, e1009733. https://doi.org/10.1371/journal.ppat.1009733.
17. Yang, K., Huang, Q., Wang, R., Zeng, Y., Cheng, M., Xue, Y., Shi, C., Ye, L., Yang, W., Jiang, Y., et al. (2021). African swine fever virus MGF505-11R inhibits type I interferon production by negatively regulating the cGAS-STING-mediated signaling pathway. Vet. Microbiol. *263*, 109265. https://doi.org/10.1016/j.vetmic.2021.109265.
18. Wang, Y., Cui, S., Xin, T., Wang, X., Yu, H., Chen, S., Jiang, Y., Gao, X., Jiang, Y., Guo, X., et al. (2021). African Swine Fever Virus MGF360-14L Negatively Regulates Type I Interferon Signaling by Targeting IRF3. Front. Cell. Infect. Microbiol. *11*, 818969. https://doi.org/10.3389/fcimb.2021.818969.
19. Zhuo, Y., Guo, Z., Ba, T., Zhang, C., He, L., Zeng, C., and Dai, H. (2021). African Swine Fever Virus MGF360-12L Inhibits Type I Interferon Production by Blocking the Interaction of Importin alpha and NF-kappaB Signaling Pathway. Virol. Sin. *36*, 176–186. https://doi.org/10.1007/s12250-020-00304-4.
20. Zhang, K., Yang, B., Shen, C., Zhang, T., Hao, Y., Zhang, D., Liu, H., Shi, X., Li, G., Yang, J., et al. (2022). MGF360-9L Is a Major Virulence Factor Associated with the African Swine Fever Virus by Antagonizing the JAK/STAT Signaling Pathway. mBio *13*, e0233021.
21. Huang, L., Xu, W., Liu, H., Xue, M., Liu, X., Zhang, K., Hu, L., Li, J., Liu, X., Xiang, Z., et al. (2021). African Swine Fever Virus pI215L Negatively Regulates cGAS-STING Signaling Pathway through Recruiting RNF138 to Inhibit K63-Linked Ubiquitination of TBK1. J. Immunol. *207*, 2754–2769. https://doi.org/10.4049/jimmunol.2100320.
22. Liu, H., Zhu, Z., Feng, T., Ma, Z., Xue, Q., Wu, P., Li, P., Li, S., Yang, F., Cao, W., et al. (2021). African Swine Fever Virus E120R Protein Inhibits Interferon Beta Production by Interacting with IRF3 To Block Its Activation. J. Virol. *95*, e0082421. https://doi.org/10.1128/JVI.00824-21.
23. Wang, X., Wu, J., Wu, Y., Chen, H., Zhang, S., Li, J., Xin, T., Jia, H., Hou, S., Jiang, Y., et al. (2018). Inhibition of cGAS-STING-TBK1 signaling pathway by DP96R of ASFV China 2018/1. Biochem. Biophys. Res. Commun. *506*, 437–443. https://doi.org/10.1016/j.bbrc.2018.10.103.
24. Ran, Y., Li, D., Xiong, M.G., Liu, H.N., Feng, T., Shi, Z.W., Li, Y.H., Wu, H.N., Wang, S.Y., Zheng, H.X., and Wang, Y.Y. (2022). African swine fever virus I267L acts as an important virulence factor by inhibiting RNA polymerase III-RIG-I-mediated innate immunity. PLoS Pathog. *18*, e1010270. https://doi.org/10.1371/journal.ppat.1010270.
25. Li, T., Zhao, G., Zhang, T., Zhang, Z., Chen, X., Song, J., Wang, X., Li, J., Huang, L., Wen, L., et al. (2021). African Swine Fever Virus pE199L Induces Mitochondrial-Dependent Apoptosis. Viruses *13*, 2240. https://doi.org/10.3390/v13112240.
26. Zhou, P., Li, L.F., Zhang, K., Wang, B., Tang, L., Li, M., Wang, T., Sun, Y., Li, S., and Qiu, H.J. (2022). Deletion of the H240R Gene of African Swine Fever Virus Decreases Infectious Progeny Virus Production Due to Aberrant Virion Morphogenesis and Enhances Inflammatory Cytokine Expression in Porcine Macrophages. J. Virol. *96*, e0030822.
27. Johnson, C.H., Ivanisevic, J., and Siuzdak, G. (2016). Metabolomics: beyond biomarkers and towards mechanisms. Nat. Rev. Mol. Cell Biol. *17*, 451–459. https://doi.org/10.1038/nrm.2016.25.
28. Johnson, C.H., Patterson, A.D., Idle, J.R., and Gonzalez, F.J. (2012). Xenobiotic metabolomics: major impact on the metabolome. Annu. Rev. Pharmacol. Toxicol. *52*, 37–56. https://doi.org/10.1146/annurev-pharmtox-010611-134748.
29. Kiseleva, O., Kurbatov, I., Ilgisonis, E., and Poverennaya, E. (2021). Defining Blood Plasma and Serum Metabolome by GC-MS. Metabolites *12*, 15. https://doi.org/10.3390/metabo12010015.
30. Lu, K., Knutson, C.G., Wishnok, J.S., Fox, J.G., and Tannenbaum, S.R. (2012). Serum metabolomics in a Helicobacter hepaticus mouse model of inflammatory bowel disease reveal important changes in the microbiome, serum peptides, and intermediary metabolism. J. Proteome Res. *11*, 4916–4926. https://doi.org/10.1021/pr300429x.
31. Xiao, N., Nie, M., Pang, H., Wang, B., Hu, J., Meng, X., Li, K., Ran, X., Long, Q., Deng, H., et al. (2021). Integrated cytokine and metabolite analysis reveals immunometabolic reprogramming in COVID-19 patients with therapeutic implications. Nat. Commun. *12*, 1618. https://doi.org/10.1038/s41467-021-21907-9.
32. Cui, L., Pang, J., Lee, Y.H., Ooi, E.E., Ong, C.N., Leo, Y.S., and Tannenbaum, S.R. (2018). Serum metabolome changes in adult patients with severe dengue in the critical and recovery phases of dengue infection. PLoS Negl. Trop. Dis. *12*, e0006217. https://doi.org/10.1371/journal.pntd.0006217.
33. Giron, L.B., Palmer, C.S., Liu, Q., Yin, X., Papasavvas, E., Sharaf, R., Etemad, B., Damra, M., Goldman, A.R., Tang, H.Y., et al. (2021). Non-invasive plasma glycomic and metabolic biomarkers of post-treatment control of HIV. Nat. Commun. *12*, 3922. https://doi.org/10.1038/s41467-021-24077-w.
34. Masarone, M., Troisi, J., Aglitti, A., Torre, P., Colucci, A., Dallio, M., Federico, A., Balsano, C., and Persico, M. (2021). Untargeted metabolomics as a diagnostic tool in NAFLD: discrimination of steatosis, steatohepatitis and cirrhosis. Metabolomics *17*, 12. https://doi.org/10.1007/s11306-020-01756-1.
35. Huang, H., Sun, Z., Pan, H., Chen, M., Tong, Y., Zhang, J., Chen, D., Su, X., and Li, L. (2016). Serum metabolomic signatures discriminate early liver inflammation and fibrosis stages in patients with chronic hepatitis B. Sci. Rep. *6*, 30853. https://doi.org/10.1038/srep30853.
36. Sun, X., Song, L., Feng, S., Li, L., Yu, H., Wang, Q., Wang, X., Hou, Z., Li, X., Li, Y., et al. (2018). Fatty Acid Metabolism is Associated With Disease Severity After H7N9 Infection. EBioMedicine *33*, 218–229. https://doi.org/10.1016/j.ebiom.2018.06.019.
37. Gong, W., Jia, J., Zhang, B., Mi, S., Zhang, L., Xie, X., Guo, H., Shi, J., and Tu, C. (2017). Serum Metabolomic Profiling of Piglets Infected with Virulent Classical Swine Fever Virus. Front. Microbiol. *8*, 731. https://doi.org/10.3389/fmicb.2017.00731.

38. Xue, Q., Liu, H., Zhu, Z., Yang, F., Song, Y., Li, Z., Xue, Z., Cao, W., Liu, X., and Zheng, H. (2022). African Swine Fever Virus Regulates Host Energy and Amino Acid Metabolism To Promote Viral Replication. J. Virol. *96*, e0191921.
39. Tran, X.H., Le, T.T.P., Nguyen, Q.H., Do, T.T., Nguyen, V.D., Gay, C.G., Borca, M.V., and Gladue, D.P. (2021). African swine fever virus vaccine candidate ASFV-G-DeltaI177L efficiently protects European and native pig breeds against circulating Vietnamese field strain. Transbound. Emerg. Dis. *69*, e494–e504. https://doi.org/10.1111/tbed.14329.
40. Liu, P., Yin, Y., Gong, Y., Qiu, X., Sun, Y., Tan, L., Song, C., Liu, W., Liao, Y., Meng, C., and Ding, C. (2019). In Vitro and In Vivo Metabolomic Profiling after Infection with Virulent Newcastle Disease Virus. Viruses *11*, 962. https://doi.org/10.3390/v11100962.
41. Ai, Q., Lin, X., Xie, H., Li, B., Liao, M., and Fan, H. (2021). Proteome Analysis in PAM Cells Reveals That African Swine Fever Virus Can Regulate the Level of Intracellular Polyamines to Facilitate Its Own Replication through ARG1. Viruses *13*, 1236. https://doi.org/10.3390/v13071236.
42. Hu, M.-M., He, W.-R., Gao, P., Yang, Q., He, K., Cao, L.-B., Li, S., Feng, Y.-Q., and Shu, H.-B. (2019). Virus-induced accumulation of intracellular bile acids activates the TGR5-β-arrestin-SRC axis to enable innate antiviral immunity. Cell Res. *29*, 193–205. https://doi.org/10.1038/s41422-018-0136-1.
43. Xue, H., Gan, F., Zhang, Z., Hu, J., Chen, X., and Huang, K. (2015). Astragalus polysaccharides inhibits PCV2 replication by inhibiting oxidative stress and blocking NF-kappaB pathway. Int. J. Biol. Macromol. *81*, 22–30. https://doi.org/10.1016/j.ijbiomac.2015.07.050.
44. Patti, G.J., Yanes, O., and Siuzdak, G. (2012). Innovation: Metabolomics: the apogee of the omics trilogy. Nat. Rev. Mol. Cell Biol. *13*, 263–269. https://doi.org/10.1038/nrm3314.
45. Manchester, M., and Anand, A. (2017). Metabolomics: Strategies to Define the Role of Metabolism in Virus Infection and Pathogenesis. Adv. Virus Res. *98*, 57–81. https://doi.org/10.1016/bs.aivir.2017.02.001.
46. Meng, H., Sun, M., Jiang, Z., Liu, Y., Sun, Y., Liu, D., Jiang, C., Ren, M., Yuan, G., Yu, W., et al. (2021). Comparative transcriptome analysis reveals resistant and susceptible genes in tobacco cultivars in response to infection by Phytophthora nicotianae. Sci. Rep. *11*, 809. https://doi.org/10.1038/s41598-020-80280-7.
47. Juárez Olguín, H., Calderón Guzmán, D., Hernández García, E., and Barragán Mejía, G. (2016). The Role of Dopamine and Its Dysfunction as a Consequence of Oxidative Stress. Oxid. Med. Cell. Longev. *2016*, 9730467. https://doi.org/10.1155/2016/9730467.
48. Basova, L.V., Lindsey, A., McGovern, A., Rosander, A., Delorme-Walker, V., ElShamy, W.M., Pendyala, V.V., Gaskill, P.J., Ellis, R.J., Cherner, M., et al. (2023). MRP8/14 Is a Molecular Signature Triggered by Dopamine in HIV Latent Myeloid Targets That Increases HIV Transcription and Distinguishes HIV+ Methamphetamine Users with Detectable CSF Viral Load and Brain Pathology. Viruses *15*, 1363. https://doi.org/10.3390/v15061363.
49. Limanaqi, F., Zecchini, S., Dino, B., Strizzi, S., Cappelletti, G., Utyro, O., Vanetti, C., Garziano, M., Saulle, I., Clerici, M., and Biasin, M. (2022). Dopamine Reduces SARS-CoV-2 Replication In Vitro through Downregulation of D2 Receptors and Upregulation of Type-I Interferons. Cells *11*, 1691. https://doi.org/10.3390/cells11101691.
50. Mpekoulis, G., Tsopela, V., Panos, G., Siozos, V., Kalliampakou, K.I., Frakolaki, E., Sideris, C.D., Vassiliou, A.G., Sideris, D.C., Vassilacopoulou, D., and Vassilaki, N. (2021). Association of Hepatitis C Virus Replication with the Catecholamine Biosynthetic Pathway. Viruses *13*, 2139. https://doi.org/10.3390/v13112139.
51. Frakolaki, E., Kalliampakou, K.I., Kaimou, P., Moraiti, M., Kolaitis, N., Boleti, H., Koskinas, J., Vassilacopoulou, D., and Vassilaki, N. (2019). Emerging Role of l-Dopa Decarboxylase in Flaviviridae Virus Infections. Cells *8*, 837. https://doi.org/10.3390/cells8080837.
52. Channer, B., Matt, S.M., Nickoloff-Bybel, E.A., Pappa, V., Agarwal, Y., Wickman, J., Gaskill, P.J., and Khoshbouei, H. (2023). Dopamine, Immunity, and Disease. Pharmacol. Rev. *75*, 62–158. https://doi.org/10.1124/pharmrev.122.000618.
53. Guo, Y., Zhang, X.-N., Su, S., Ruan, Z.-L., Hu, M.-M., and Shu, H.-B. (2023). β-adrenoreceptor-triggered PKA activation negatively regulates the innate antiviral response. Cell. Mol. Immunol. *20*, 175–188. https://doi.org/10.1038/s41423-022-00967-x.
54. Lagunoff, M. (2016). Activation of cellular metabolism during latent Kaposi's Sarcoma herpesvirus infection. Curr. Opin. Virol. *19*, 45–49. https://doi.org/10.1016/j.coviro.2016.06.012.
55. Singh, R.K., Lang, F., Pei, Y., Jha, H.C., and Robertson, E.S. (2018). Metabolic reprogramming of Kaposi's sarcoma associated herpes virus infected B-cells in hypoxia. PLoS Pathog. *14*, e1007062. https://doi.org/10.1371/journal.ppat.1007062.
56. Chandler, J.D., Hu, X., Ko, E.J., Park, S., Lee, Y.T., Orr, M., Fernandes, J., Uppal, K., Kang, S.M., Jones, D.P., and Go, Y.M. (2016). Metabolic pathways of lung inflammation revealed by high-resolution metabolomics (HRM) of H1N1 influenza virus infection in mice. Am. J. Physiol. Regul. Integr. Comp. Physiol. *311*, R906–R916. https://doi.org/10.1152/ajpregu.00298.2016.
57. Cui, L., Zheng, D., Lee, Y.H., Chan, T.K., Kumar, Y., Ho, W.E., Chen, J.Z., Tannenbaum, S.R., and Ong, C.N. (2016). Metabolomics Investigation Reveals Metabolite Mediators Associated with Acute Lung Injury and Repair in a Murine Model of Influenza Pneumonia. Sci. Rep. *6*, 26076. https://doi.org/10.1038/srep26076.
58. Bernatchez, J.A., and McCall, L.I. (2020). Insights gained into respiratory infection pathogenesis using lung tissue metabolomics. PLoS Pathog. *16*, e1008662. https://doi.org/10.1371/journal.ppat.1008662.
59. Sabariegos, R., Ortega-Prieto, A.M., Díaz-Martínez, L., Grande-Pérez, A., García Crespo, C., Gallego, I., de Ávila, A.I., Albentosa-González, L., Soria, M.E., Gastaminza, P., et al. (2022). Guanosine inhibits hepatitis C virus replication and increases indel frequencies, associated with altered intracellular nucleotide pools. PLoS Pathog. *18*, e1010210. https://doi.org/10.1371/journal.ppat.1010210.
60. Al-Kuraishy, H.M., Al-Gareeb, A.I., Al-Niemi, M.S., Aljowaie, R.M., Almutairi, S.M., Alexiou, A., and Batiha, G.E.S. (2022). The Prospective Effect of Allopurinol on the Oxidative Stress Index and Endothelial Dysfunction in Covid-19. Inflammation *45*, 1651–1667. https://doi.org/10.1007/s10753-022-01648-7.
61. Carrascosa, A.L., Santarén, J.F., and Viñuela, E. (1982). Production and titration of African swine fever virus in porcine alveolar macrophages. J. Virol. Methods *3*, 303–310. https://doi.org/10.1016/0166-0934(82)90034-9.
62. Schmittgen, T.D., and Livak, K.J. (2008). Analyzing real-time PCR data by the comparative C(T) method. Nat. Protoc. *3*, 1101–1108. https://doi.org/10.1038/nprot.2008.73.

STAR★METHODS

KEY RESOURCES TABLE

REAGENT or RESOURCE	SOURCE	IDENTIFIER
Antibodies		
Anti-P72 (B646L) polyclonal antibodies	This paper	N/A
Anti-P30 (CP204L) polyclonal antibodies	This paper	N/A
Rabbit polyclonal anti-beta actin antibody	Proteintech	Cat#20536-1-AP; RRID:AB_10700003
Bacterial and virus strains		
ASFV CN/GS/2018	Lanzhou Veterinary Research Institute	N/A
Biological samples		
Serum from ASFV infected pigs	This paper	N/A
Serum from healthy pigs	This paper	N/A
Chemicals, peptides, and recombinant proteins		
L741626	Sigma-Aldrich	505879; CAS:81226-60-0
R (+)-SCH-23390	Sigma-Aldrich	D054; CAS:125941-87-9
L-dopa	Sigma-Aldrich	333786; CAS:53587-29-4
Guanosine	Sigma-Aldrich	G6264; CAS:118-00-3
Allopurinol	Sigma-Aldrich	A 8003; CAS:315-30-0
Deposited data		
Metabolomics data	Mendeley Data	https://doi.org/10.17632/7bsjsbdcg7.1
Experimental models: Cell lines		
Porcine alveolar macrophages	Prepared from pigs (Carrascosa AL. et al.[61])	N/A
Oligonucleotides		
Primer P72 Forward: 5′-GCGCTCTGGATTAAGTTGCG-3′	This paper	N/A
Primer P72 reverse: 5′-ATATTGCGTCTACTGGG GCG-3′	This paper	N/A
Primer GAPDH forward: 5′ACATGGCCTCCAAGGAGTAAGA-3′	This paper	N/A
Primer GAPDH reverse: 5′GCGAGTTGGGGCTGTG ACT-3′	This paper	N/A
Software and algorithms		
SIMCA-P 14.1	Sartorius Stedim Data Analytics AB	N/A
GraphPad Prism 8	GraphPad Software	https://www.graphpad.com/
XCMS	XCMS Software	https://xcmsonline.scripps.edu/index.php

RESOURCE AVAILABILITY

Lead contact

Further information and requests for resources and reagents should be directed to and will be fulfilled by the lead contact, Keshan Zhang (zks009@126.com).

Materials availability

This study did not generate new unique reagents.

Data and code availability

All relevant data is available in the main text and supplementary tables. The metabolomics data in this paper were deposited on Mendeley at [https://doi.org/10.17632/7bsjsbdcg7.1]. This paper does not report original code. Any additional information required to reanalyze the data reported in this paper is available from the lead contact upon request.

EXPERIMENTAL MODEL AND STUDY PARTICIPANT DETAILS

Cells

Porcine alveolar macrophages (PAMs) were prepared as previously described,[61] and cultured in Roswell Park Memorial Institute 1640 medium containing 10% porcine serum at 37°C under 5% CO_2.

Animal experiments and samples collection

All animal experiments were carried out in strict accordance with good animal practice according to the Animal Ethics Procedures and Guidelines of the People's Republic of China, and the study was approved by the Animal Ethics Committee of Lanzhou Veterinary Research Institute, Chinese Academy of Agricultural Sciences.

All animal experiments were performed in the enhanced biosafety level 3 (P3) facilities in Lanzhou Veterinary Research Institute (LVRI) of the Chinese Academy of Agricultural Sciences (CAAS) approved by the Ministry of Agriculture and Rural Affairs and China National Accreditation Service for Conformity Assessment.

Landrace pigs (female, approximately 75 days old and 30–35 kg weight, n=8), free of porcine reproductive and respiratory syndrome virus (PRRSV), pseudorabies virus (PRV), porcine epidemic diarrhea virus (PEDV) and porcine circovirus type 2 (PCV-2), were obtained from a high-health farm. The pigs and were allowed free access to standard diet and water.

Pigs in the infected groups were injected with ASFV CN/GS/2018 (1 HAD50). The serum samples were collection from all pigs at days 0 (before injection), 5, 10 post infection (dpi) and stored at -80°C for metabolomics analysis.

METHOD DETAILS

Metabolite extraction

Take out the sample from the -80°C refrigerator and thaw it on ice, 20 mg of sample was mix with 400 μL 70% methanol water internal standard extractant homogenize with a steel ball using a ball mill at 30 HZ for 20 s, then centrifuged at 3000 rpm for 30 s at 4°C. Subsequently, add 400 μL of 70% methanol water internal standard extractant, shook 5 min with 1500 rpm and placed on ice for 15 min. The samples were centrifuged at 12000 rpm for 10 min at 4°C, the supernatant (300 μL) was transferred to a new Eppendorf tube and incubated at -20°C for 30 min. Finally, the samples were centrifuged at 12000 rpm for 3min at 4°C, and take the supernatant for further analysis.

UHPLC-TQMS analysis

The collected supernatant, 2ul sample volume, was injected into a 100 × 2.1 mm^2, 1.8 μm HSS T3 column (Waters, Milford, MA) held at 40°C using an Agilent 1290 Infinity UPLC system (ExionLC AD). The mobile phase consisted of A (water, containing 0.1% formic acid) and B (acetonitrile, containing 0.1% formic acid). The gradient elution procedure was as followes: 95:5 A/B at 0 min, 10:90 A/B at 10.0 min, 10:90 A/B at 11.0 min, 95:5 A/B at 11.1 min, 95:5 A/B at 14.0 min. The flow rate was 0.4 ml/min.

The AB Triple TOF 6600 mass spectrometer (AB SCIEX, USA) was used for its ability to acquire MS/MS spectra on an information dependent basis (IDA). In this mode, the acquisition software (TripleTOF 6600, AB SCIEX) continuously evaluates the full scan survey MS data as it collects and triggers the acquisition of MS/MS spectra depending on preselected criteria. In each cycle, 12 precursor ions whose intensity greater than 100 were chosen for fragmentation at collision energy (CE) of 30 V (12 MS/MS with product ion accumulation time of 50 msec each). Electrospray ionization (ESI) worked in positive and negative ion modes, The parameters were set as follows: ion source gas 1 as 50 Psi, ion source gas 2 as 50 Psi, curtain gas as 25 Psi, source temperature 500°C, ion Spray voltage floating (ISVF) 5500 V or -4500 V in positive or negative modes, respectively.

Western blotting

For western blotting, the prepared protein samples were loaded onto an SDS-PAGE gel (10%) and were transferred onto a nitrocellulose membrane (EMD Millipore, Billerica, MA, USA). Then, the membrane was blocked for 2 h at room temperature and incubated overnight at 4°C with the following primary antibodies: anti-P30 (1:1000), anti-P72 (1:1000), and anti-β-actin (1:5000, Proteintech, Chicago, USA). Appropriate secondary antibodies were selected to incubate with the membrane for 2 h at room temperature. Finally, blot bands were visualized with an ECL reagent (Advansta, California, USA) using Odyssey infrared imaging system.

Real-time quantitative polymerase chain reaction (qPCR)

To analysis the mRNA expression of ASFV gene. Total RNA was extracted from PAMs cells using RNA extraction kit (Biogoethe Biotechnology Co., Ltd, Wuhan) according to the manufacturer's protocol. Then, total RNA was reverse transcribed into cDNA using the PrimeScript RT kit (TaKaRa, Beijing). The qPCR was performed using the generated cDNA and TB green Premix Ex Taq reagent on the ABI StepOnePlus system. The target gene of ASFV for amplification was P72 gene, whose amplification primers were P72F and P72R (P72F: 5′-GCGCTCTGGATT AAGTTGCG-3′; P72R: 5′-ATATTGCGTCTACTGGG GCG-3′). Glyceraldehyde-3-phosphate dehydrogenase (GAPDH) gene was used as the internal control (Primer: GAPDH-F: 5′ACATGGCCTCCAAGGAGTAAGA-3′; GAPDH-R: 5′GCGAGTTGGGGCTGTG ACT-3′). Finally, the relative expression of P72 mRNA was calculated based on the comparative cycle threshold ($2^{-\Delta\Delta CT}$) method.[62]

QUANTIFICATION AND STATISTICAL ANALYSIS

For metabolomics analysis, the peak alignment, calibration, retention time, and peak area of raw data were extracted using XCMS software (https://xcmsonline.scripps.edu/index.php). To assess the changes in the levels of small-molecule metabolites after ASFV infection, unsupervised principal component analysis (PCA) and orthogonal partial least-squares discriminant analysis (OPLS–DA) were performed using SIMCA-P 14.1 software package. The quality of OPLS–DA models was described using R^2X and Q^2 values. In addition, the identified metabolites were annotated using the Kyoto Encyclopedia of Genes and Genomes (KEGG) to identify the metabolic pathways that were altered during ASFV infection.

All *in vitro* experiments were repeated three times. The data are presented as the mean ± standard deviation (SD) and the significance of data between groups was analyzed using GraphPad Prism v.8 (San Diego, CA, USA). * $P < 0.05$, ** $P < 0.01$, and *** $P < 0.001$ were considered statistically significant.